Supporting Information

Selective hydrogenolysis of glycerol to 1,3-propanediol over rhenium oxide-modified iridium nanoparticles coating rutile titania support

Lujie Liu,[a] Takehiro Asano,[a] Yoshinao Nakagawa,[a,b,*] Masazumi Tamura,[a,b]

Kazu Okumura[c] and Keiichi Tomishige[a,b,*]

[a] *Department of Applied Chemistry, School of Engineering, Tohoku University,*

6-6-07 Aoba, Aramaki, Aoba-ku, Sendai, 980-8579, Japan

[b] *Research Center for Rare Metal and Green Innovation, Tohoku University,*

468-1, Aoba, Aramaki, Aoba-ku, Sendai 980-0845, Japan

[c] *Department of Applied Chemistry, Faculty of Engineering, Kogakuin University,*

2665-1 Nakano-machi, Hachioji, Tokyo 192-0015, Japan

* Corresponding authors.

School of Engineering, Tohoku University,

6-6-07, Aoba, Aramaki, Aoba-ku, Sendai, 980-8579, Japan

E-mail: yoshinao@erec.che.tohoku.ac.jp, Tel/Fax: +81-22-795-7215 (Y. N.);

tomi@erec.che.tohoku.ac.jp, Tel/Fax: +81-22-795-7214 (K. T.)

Contents

Description of EXAFS measurement

Supporting figures

573) or reaction. (I) k^3-Weighted EXAFS oscillations. (II) Fourier transform of k^3-weighted Re L_3-edge EXAFS, FT range: 30-120 nm^{-1}. (III) Fourier filtered EXAFS data (solid line) and calculated data (dotted line), Fourier filtering range: 0.150-0.313 nm. (a) Re powder, (b) NH_4ReO_4, (c) 4 wt%-Ir, Re/Ir = 0.08*, (d) 4 wt%-Ir, Re/Ir = 0.12*, (e) 4 wt%-Ir, Re/Ir = 0.24*, (f) 4 wt%-Ir, Re/Ir = 0.24* after reaction, (g) 4 wt%-Ir, Re/Ir = 0.25*, (h) 4 wt%-Ir, Re/Ir = 0.30*, (i) 4 wt%-Ir, Re/Ir = 0.30* after reaction, (j) 4 wt%-Ir Ir-ReO_x/SiO_2 (Re/Ir = 1) after reaction with H_2SO_4 addition (H^+/Ir = 1), Ref. S4, Fourier filtering range: 0.156-0.331 nm. (k) 2 wt%-Ir Ir-ReO_x/Rutile (Re/Ir = 0.32*) (G, 573), (l) 6 wt%-Ir Ir-ReO_x/Rutile (Re/Ir = 0.18*) (G, 573), (m) 8 wt%-Ir Ir-ReO_x/Rutile (Re/Ir = 0.15*) (G, 573).

Supporting tables

Table S1 Summary of previous reports on hydrogenolysis of glycerol to 1,3-PrD over Pt-WO_x based, Ir-Re based, and the present catalysts using water as solvent

Table S2 Summary of precursors, gases, supports and reagents used in this work

Table S3 Effect of H_2 pressure on glycerol hydrogenolysis over 4 wt%-Ir Ir-ReO_x/Rutile (Re/Ir = 0.24*)

Table S4 Effect of glycerol concentration on glycerol hydrogenolysis over 4 wt% Ir-ReO_x/Rutile (Re/Ir = 0.24*)

Table S5 Reusability of 4 wt%-Ir Ir-ReO_x/Rutile

Table S6 Valence of Re determined by H_2 consumption and XRF

Table S7 Results of FT-IR of adsorbed CO analysis over Ir/Rutilr and Ir-ReO_x/Rutile catalysts

Table S8 Dependency of Re/Ir ratio on glycerol to 1,3-PrD over Ir-ReO_x/Rutile

References

Description of EXAFS measurement

The X-ray absorption near edge structure (XANES) and extended X-ray absorption fine structure (EXAFS) spectra measurements were carried out at the BL01B1 and BL14B2 stations at SPring-8. The storage ring was operated at 8 GeV, and a monochromatic X-ray beam was obtained by using a Si (1 1 1) single crystal. For Re L_3-edge and Ir L_3-edge measurement, two ion chambers for I_0 and I were filled with 85% N_2 + 15% Ar and 50% N_2 + 50% Ar, respectively. For analysis, the extracted oscillation was obtained using a spline smoothing approach from the original EXAFS data [S1]. A radial distribution function was obtained after Fourier transformation of the k^3-weighted EXAFS oscillation from the k space to the r space was accomplished. A usual curve fitting approach was used for analyzing the inversely Fourier filtered data [S2, S3]. The empirical phase shift and amplitude functions for the Re–O and Ir–O bonds were extracted from the data of NH_4ReO_4 and IrO_2, respectively. It is very difficult to distinguish between Ir and Re as a scattering atom. Therefore, the empirical phase shift and amplitude functions for the Ir–Ir and Ir–Re bonds were extracted from the data of Ir powder, and for those of Re–Re, and Re–Ir bonds were extracted from the data of Re powder. The Re–Ir and Ir–Ir bonds are represented by the Re–Ir (or –Re) and Ir–Ir (or –Re) in the curve fitting results. Analyses of XANES and EXAFS data were performed using a computer program (REX2000, ver. 2.6; Rigaku Corp.).

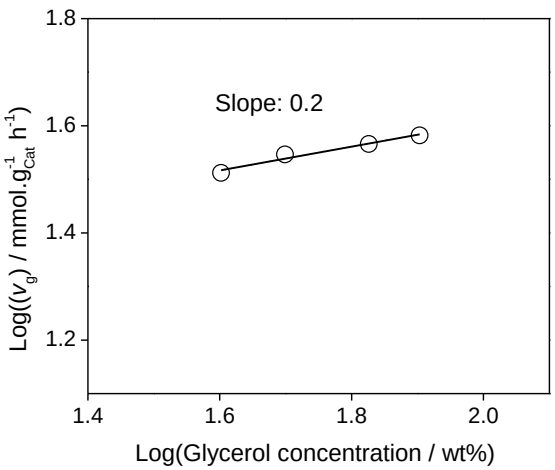

Figure S1. Kinetics study of effect of glycerol concentration on glycerol hydrogenolysis over 4 wt%-Ir Ir-ReO_x/Rutile (Re/Ir = 0.24*) at around standard reaction conditions (glycerol concentration: 40~80 wt%). Details of reaction conditions and results are summarized in Table S4. Reduction conditions: H_2 flow at 573 K (G, 573).

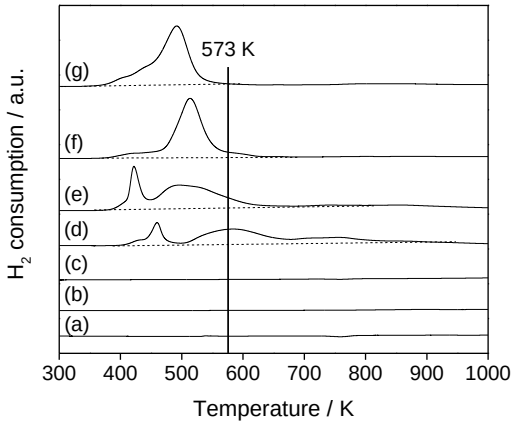

Figure S2. TPR profiles of TiO_2 support and 4 wt%-Ir Ir-ReO_x/TiO_2, (a) P25 TiO_2, (b) anatase TiO_2, (c) rutile TiO_2, (d) 4 wt% Ir/P25, (e) 4 wt%-Ir Ir-ReO_x/P25 (Re/Ir = 0.30*), (f) 4 wt% Ir/Anatase, (g) 4 wt%-Ir Ir-ReO_x/Anatase (Re/Ir = 0.16*). Y-axis was normalized by the weight of catalysts. Conditions: H_2/Ar (5% v/v, 30 cm^3 min^{-1}) at heating rate of 10 K min^{-1}. Dotted line represents the baseline for H_2 consumption amount calculation.

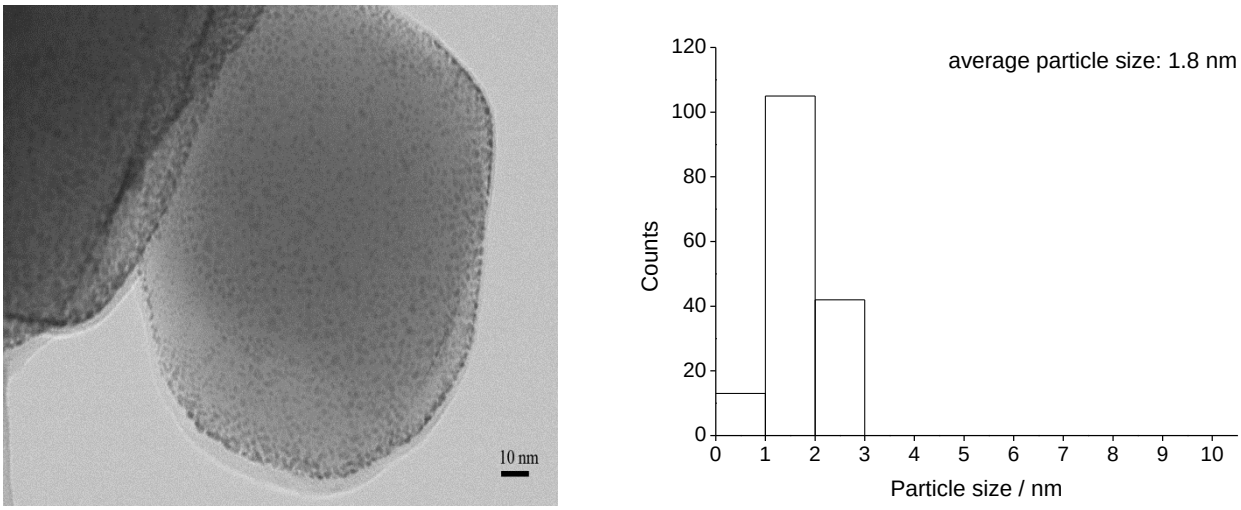

Figure S3. TEM images of Ir-ReO_x/Rutile (G, 573). Ir: 4 wt%, Re/Ir = 0.3* (1).

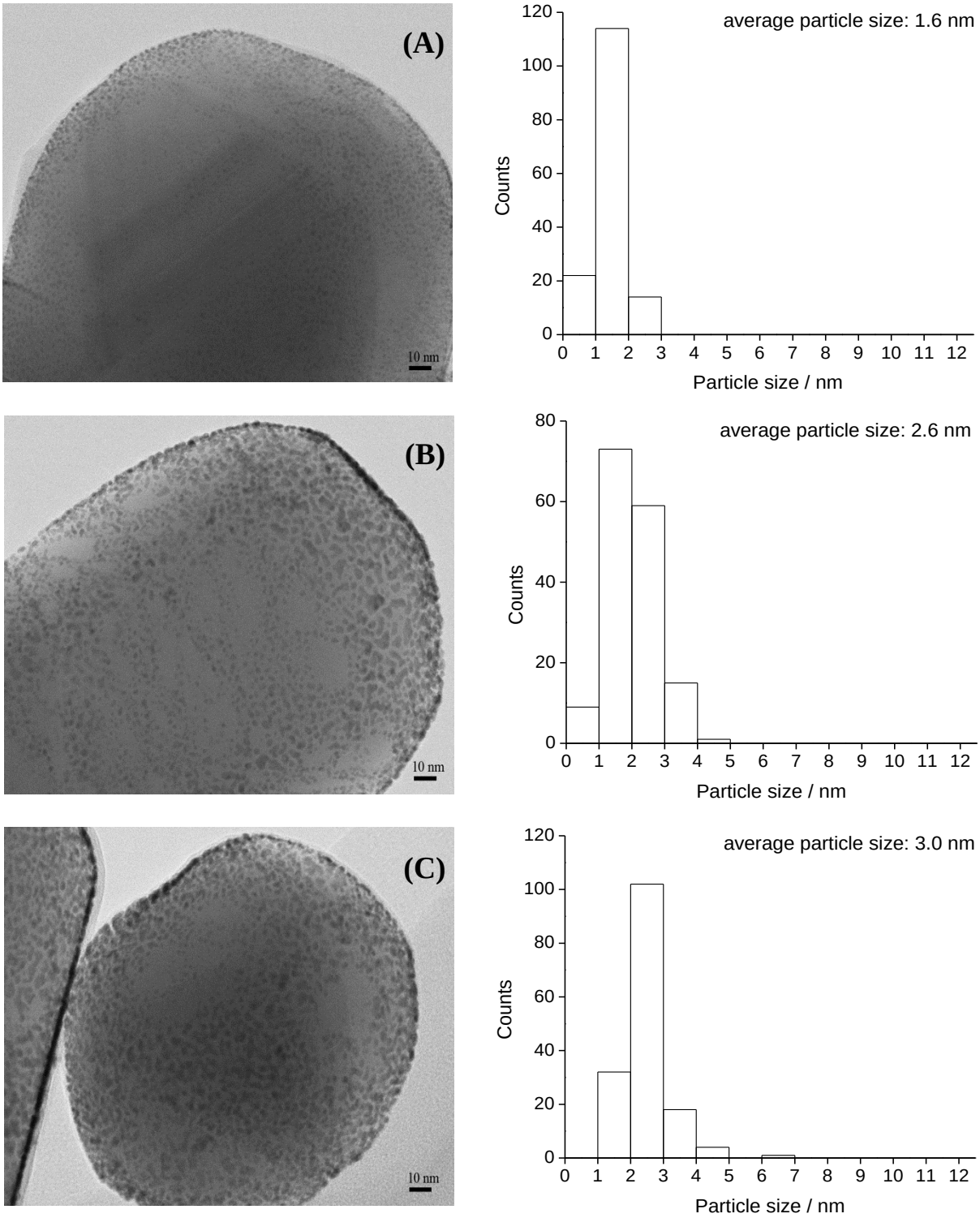

Figure S4. TEM images of catalysts: (A) 2 wt%-Ir Ir-ReO_x/Rutile, (B) 6 wt%-Ir Ir-ReO_x/Rutile, (C) 8 wt%-Ir Ir-ReO_x/Rutile. Re/Ir = 0.25. Catalysts were pre-reduced by H_2 at 573 K for 1 h before measurement.

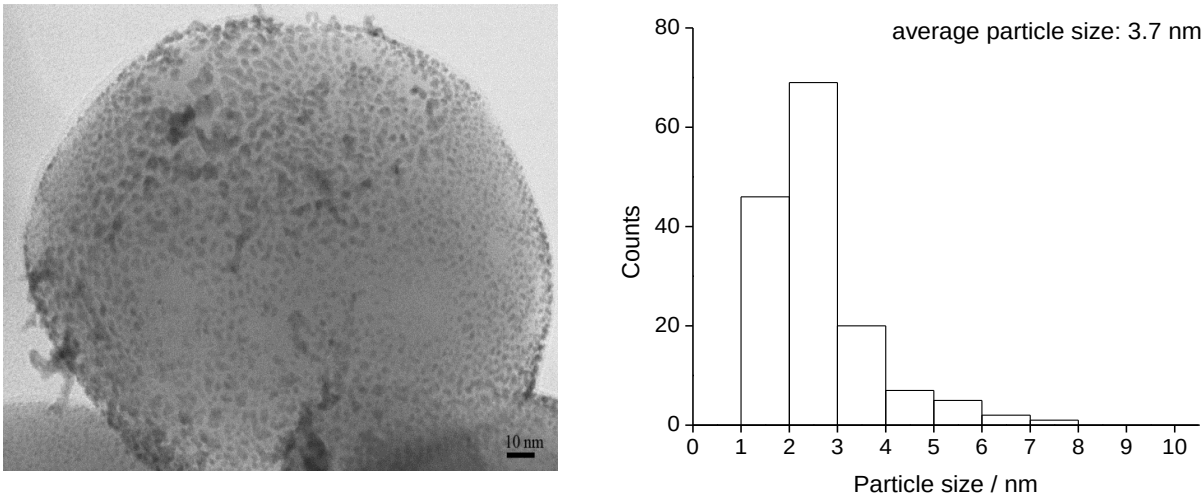

Figure S5. TEM images of Ir-ReO_x/Rutile (G, 573). Ir: 4 wt% (precursor of $Ir(NO_3)_4$), Re/Ir = 0.27* (0.25).

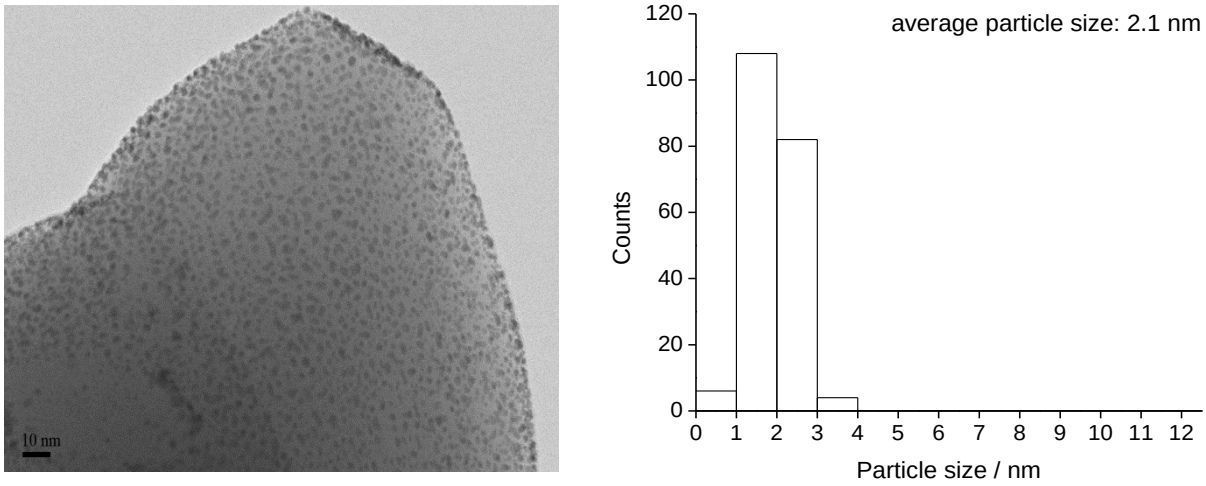

Figure S6. TEM images of catalysts: Ir-ReO_x/Rutile (G, 773). Ir: 4 wt%, Re/Ir = 0.24* (0.25).

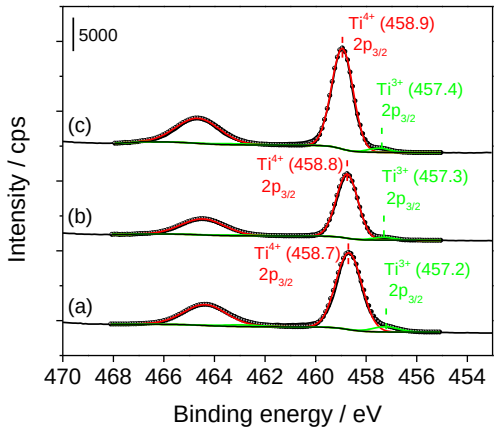

Figure S7. XPS fitting results of Ti over 4 wt%-Ir Ir-ReO_x/Rutile reduced at 573 K. (a) Ir/Rutile, (b) Re/Ir = 0.24*, (c) Re/Ir = 0.3*.

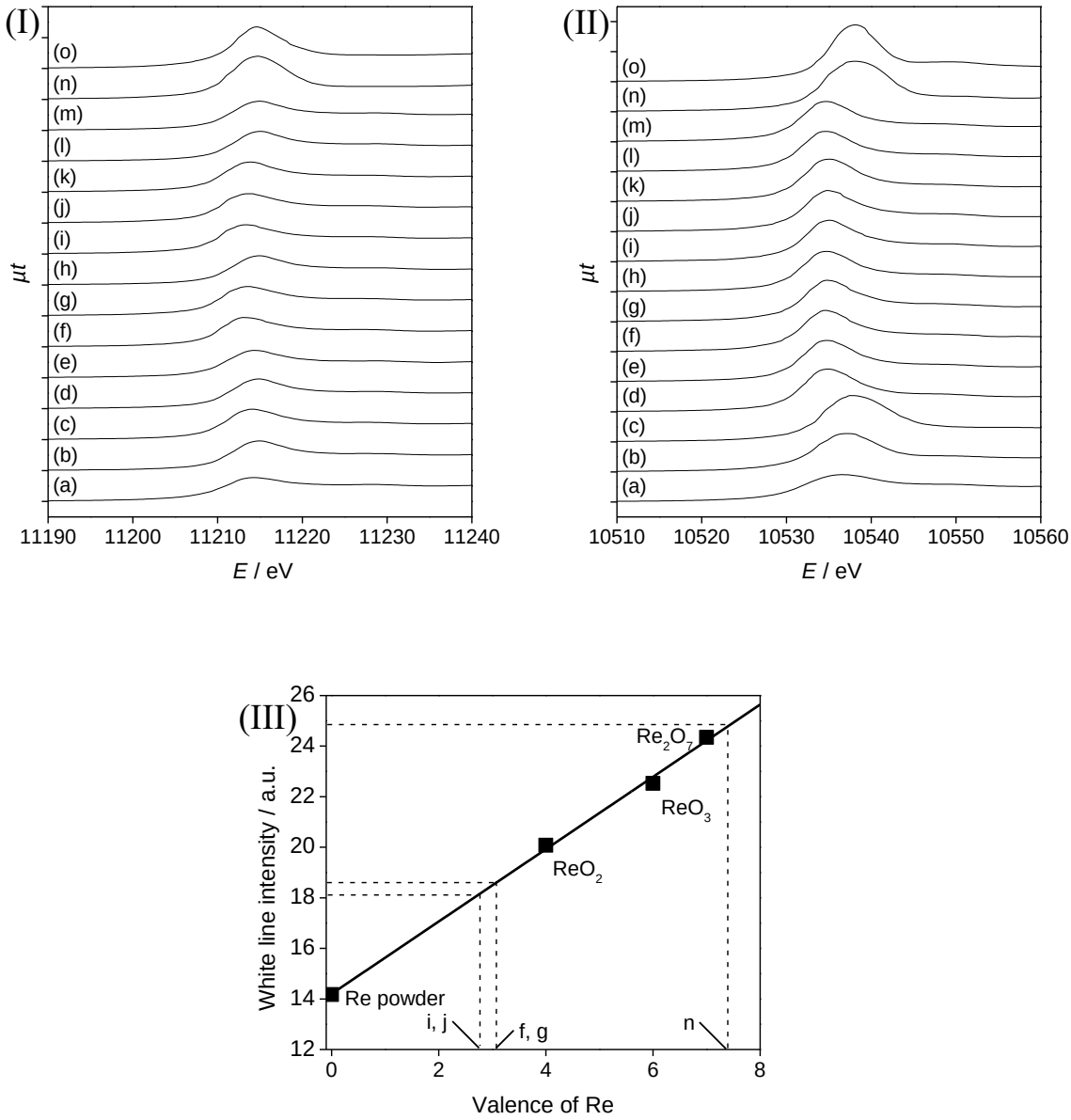

Figure S8. Results of Ir L_3-edge and Re L_3-edge XANES analysis of 4 wt% Ir/Rutile and Ir-ReO_x/Rutile catalysts after gas-phase reduction (G, 573) or reaction. (I) Ir L_3-edge XANES spectra of (a) Ir powder, (b) Ir/Rutile, (c) Ir/Rutile after reaction, (d) 4 wt%-Ir, Re/Ir = 0.08*, (e) 4 wt%-Ir, Re/Ir = 0.12*, (f) 4 wt%-Ir, Re/Ir = 0.24*, (g) 4 wt%-Ir, Re/Ir = 0.24* after reaction, (h) 4 wt%-Ir, Re/Ir = 0.25*, (i) 4 wt%-Ir, Re/Ir = 0.30*, (j) 4 wt%-Ir, Re/Ir = 0.30* after reaction, (k) 2 wt%-Ir, Re/Ir = 0.32*, (l) 6 wt%-Ir, Re/Ir = 0.18*, (m) 8 wt%-Ir, Re/Ir = 0.15*, (n) 4 wt%-Ir, Re/Ir = 0.24* after calcination, (o) IrO_2; (II) Re L_3-edge XANES spectra of (a) Re powder, (b) ReO_2, (c) ReO_3, (d)~(m) were same to those in (I), (n) 4 wt%-Ir, Re/Ir = 0.24* after calcination, (o) Re_2O_7; (III) Typical cases of relation between white line area and valence of Re.

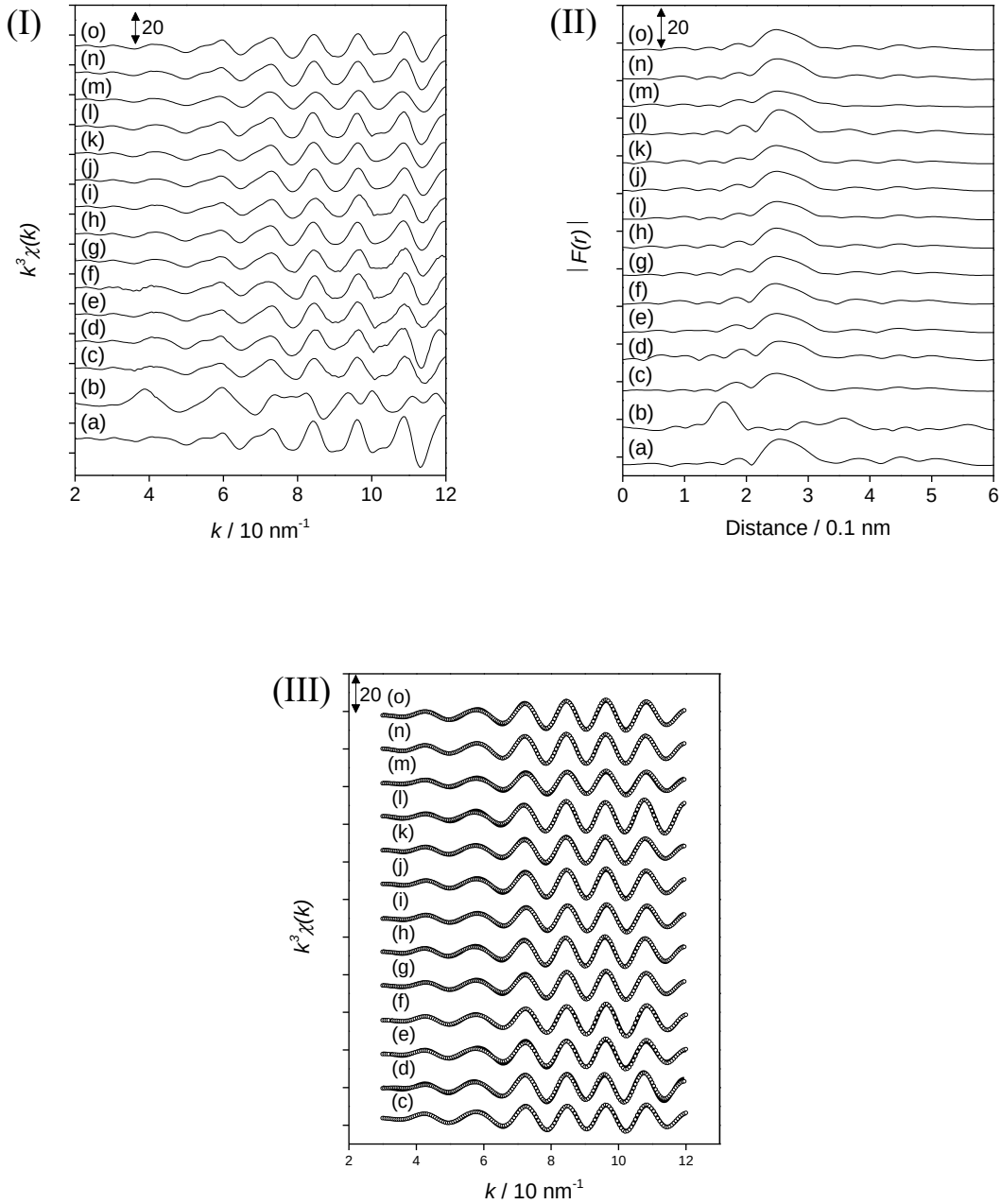

Figure S9. Results of Ir L_3-edge EXAFS analysis of 4 wt% Ir/Rutile and Ir-ReO_x/Rutile catalysts after gas-phase reduction (G, 573) or reaction. (I) k^3-Weighted EXAFS oscillations. (II) Fourier transform of k^3-weighted Ir L_3-edge EXAFS, FT range: 30-120 nm^{-1}. (III) Fourier filtered EXAFS data (solid line) and calculated data (dotted line), Fourier filtering range: 0.156-0.325 nm. (a) Ir powder, (b) IrO_2, (c) Ir/Rutile, (d) Ir/Rutile after reaction, (e) 4 wt%-Ir, Re/Ir = 0.08*, (f) 4 wt%-Ir, Re/Ir = 0.12*, (g) 4 wt%-Ir, Re/Ir = 0.24*, (h) 4 wt%-Ir, Re/Ir = 0.24* after reaction, (i) 4 wt%-Ir, Re/Ir = 0.25*, (j) 4 wt%-Ir, Re/Ir = 0.30*, (k) 4 wt%-Ir, Re/Ir = 0.30* after reaction, (l) 4 wt%-Ir Ir-ReO_x/SiO_2 (Re/Ir = 1) after reaction with H_2SO_4 addition (H^+/Ir = 1), Ref. S4, (m) 2 wt%-Ir Ir-ReO_x/Rutile (Re/Ir = 0.32*) (G, 573), (n) 6 wt%-Ir Ir-ReO_x/Rutile (Re/Ir = 0.18*) (G, 573), (o) 8 wt%-Ir Ir-ReO_x/Rutile (Re/Ir = 0.15*) (G, 573).

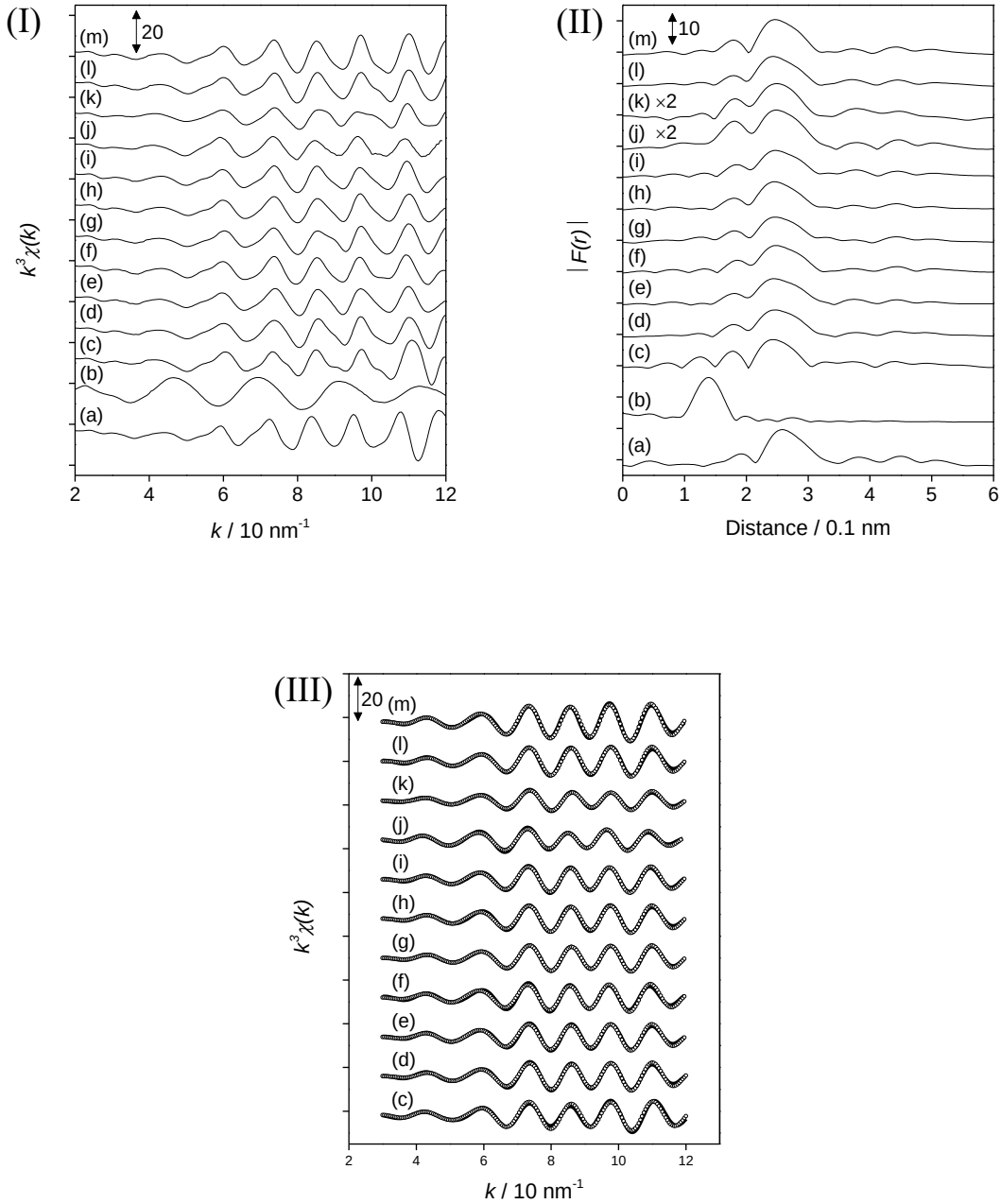

Figure S10. Results of Re L_3-edge EXAFS analysis of Ir-ReO_x/Rutile catalyst after gas-phase reduction (G, 573) or reaction. (I) k^3-Weighted EXAFS oscillations. (II) Fourier transform of k^3-weighted Re L_3-edge EXAFS, FT range: 30-120 nm^{-1}. (III) Fourier filtered EXAFS data (solid line) and calculated data (dotted line), Fourier filtering range: 0.150-0.313 nm. (a) Re powder, (b) NH_4ReO_4, (c) 4 wt%-Ir, Re/Ir = 0.08*, (d) 4 wt%-Ir, Re/Ir = 0.12*, (e) 4 wt%-Ir, Re/Ir = 0.24*, (f) 4 wt%-Ir, Re/Ir = 0.24* after reaction, (g) 4 wt%-Ir, Re/Ir = 0.25*, (h) 4 wt%-Ir, Re/Ir = 0.30*, (i) 4 wt%-Ir, Re/Ir = 0.30* after reaction, (j) 4 wt%-Ir Ir-ReO_x/SiO_2 (Re/Ir = 1) after reaction with H_2SO_4 addition (H^+/Ir = 1), Ref. S4, Fourier filtering range: 0.156-0.331 nm. (k) 2 wt%-Ir Ir-ReO_x/Rutile (Re/Ir = 0.32*) (G, 573), (l) 6 wt%-Ir Ir-ReO_x/Rutile (Re/Ir = 0.18*) (G, 573), (m) 8 wt%-Ir Ir-ReO_x/Rutile (Re/Ir = 0.15*) (G, 573).

Table S1 Summary of previous reports on hydrogenolysis of glycerol to 1,3-PrD over Pt-WO_x based, Ir-Re based, and the present catalysts using water as solvent

Entry	Catalyst	Composition		Reaction conditions		$P_{1,3\text{-PrD}}$ / (g g_{Pt}^{-1} h^{-1})	Ref.
		Pt / wt%	W/Pt molar ratio	T / K	$P(H_2)$ / MPa		
1	Pt-LiSiW/ZrO_2	1.0	(20 wt% HSiW) 18.3	453	5.0	0.2	[S5]
2	Pt/WO_x/Al_2O_3	9.0	(8 wt% W) 0.94	493	4.5	0.6	[S6]
3	Pt/WO_x/Al_2O_3	8.9	(8 wt% W) 0.95	493	4.5	1	[S7]
4	Pt/WO_3/TiO_2/SiO_2	2.0	(5 wt% WO_3) 2.1	453	5.5	1	[S8]
5	Pt/$Ti_{80}W_{20}$	2.0	(W/Ti = 20:80) -	453	5.5	1	[S9]
6	Pt/WO_x/SiO_2-ZrO_2	2.0	(15 wt% WO_3) 6.3	453	5.0	1	[S10]
7	Pt-WO_3/SBA-15	2.0	(10 wt% WO_3) 4.2	483	0.1	2	[S11]
8	Pt/W–SBA-15	3.0	0.16	423	4	2	[S12]
9	Pt/WO_x/AlOOH	1.8	(8 wt% W) 4.7	453	5.0	2	[S13]
				413	1.0	0.5	
10	Pt/WO_3/ZrO_2	3.0	(10 wt% W) 3.5	403	4.0	2	[S14]
11	Pt/WO_x/Al_2O_3	6.0	(12.9 wt% W) 2.3	453	5.0	3	[S15]
12	Pt/*meso*-WO_x	2.0	-	433	1.0	4	[S16]
				413	1.0	2	
13	Pt/ZrW38Mn3	2.0	(38 wt% W) 20.2	453	8.0	4	[S17]
14	Pt-WO_x/*t*-ZrO_2	2.0	(7.7 wt% W) 4.1	413	8.0	5	[S18]
15	Ir-Re/KIT-6 (Ir-Re alloy)	(Ir) 4.0	(Re/Ir) 1	393	8.0	no data for initial one 7 (g g_{Ir}^{-1} h^{-1}), highest yield	[S19]
16	Ir-ReO_x/SiO_2 + H_2SO_4	(Ir) 4.0	(Re/Ir) 0.83*	393	8.0	18 (g g_{Ir}^{-1} h^{-1}), initial one 6 (g g_{Ir}^{-1} h^{-1}), highest yield	[S4]
17	Ir-ReO_x/SiO_2	(Ir) 20.0	(Re/Ir) 0.34*	393	8.0	22 (g g_{Ir}^{-1} h^{-1}), initial one 7 (g g_{Ir}^{-1} h^{-1}), highest yield	[S20]
18	Ir-ReO_x/Rutile	(Ir) 4.0	(Re/Ir) 0.24*	393	8.0	52 (g g_{Ir}^{-1} h^{-1}), initial one 17 (g g_{Ir}^{-1} h^{-1}), highest yield	This work
			0.30*	393	8.0	94 (g g_{Ir}^{-1} h^{-1}), initial one (Table S8)	

Table S2 Summary of precursors, gases, supports and reagents used in this work

Precursor or reagent	Manufacturer
H_2IrCl_6	Furuya Metals Co., Ltd.
$Ir(NO_3)_4$	Furuya Metals Co., Ltd.
NH_4ReO_4	Soekawa Chemical Co., Ltd.
IrO_2	Kanto Chemical Co., Inc.
ReO_2	Strem Chemicals, Inc.
H_2	Nippon Peroxide Co., Ltd., 99.99%
N_2	Nippon Peroxide Co., Ltd., > 99%
CH_4	Japan Fine Products Corp., 22.1%, diluted with Ar, standard gas
$C_2H_6 + C_3H_8$	GL Sciences, C_2H_6 (0.997%) + C_3H_8 (1.00%), diluted with N_2, standard gas
SiO_2	G6, Fuji Silysia, calcined at 973 K for 1 h, S_{BET} 485 m^2 g^{-1}
MgO	Ube Industries, Ltd., 500A, 34 m^2 g^{-1}
CeO_2	Daiichi Kigenso Co., Ltd., HS, calcined at 873 K for 1 h, 84 m^2 g^{-1}
γ-Al_2O_3	Nippon Aerosil Co., Ltd., calcined at 973 K for 1 h, 100 m^2 g^{-1}
ZrO_2	Daiichi Kigenso Kogyo Co., Ltd., calcined at 773 K for 1 h, 62 m^2 g^{-1}
Activated carbon	Shirasagi FAC-10, Japan EnviroChemicals, Ltd., 851 m^2 g^{-1}
H-ZSM-5	JRC-Z5-90H(1), Süd-Chemie Catalysts and Catalysis Society of Japan, Si/Al_2 = 90, 270 m^2 g^{-1}
Anatase TiO_2	Wako Pure Chemical Industries, Ltd., 11 m^2 g^{-1}
Rutile TiO_2	Wako Pure Chemical Industries, Ltd., 6 m^2 g^{-1}
P25 TiO_2	Nippon Aerosil, 50 m^2 g^{-1}
Glycerol	Wako Pure Chemical Industries, Ltd., > 99%
1,3-Propanediol	Wako Pure Chemical Industries, Ltd., > 97%, standard reagent
1,2-Propanediol	Wako Pure Chemical Industries, Ltd., > 99%, standard reagent
1-Propanol	Wako Pure Chemical Industries, Ltd., > 99.5%, standard reagent
2-Propanol	Wako Pure Chemical Industries, Ltd., > 99.7%, standard reagent
1-Butanol	Wako Pure Chemical Industries, Ltd., > 99%, internal standard

Table S3 Effect of H_2 pressure on glycerol hydrogenolysis over 4 wt%-Ir Ir-ReO_x/Rutile (Re/Ir = 0.24*)

t / h	*P* / MPa	Conv. / %	Selectivity / %					Conversion rate (v_g) / mmol·g-Cat^{-1} h^{-1}
			1,3-PrD	1,2-PrD	1-PrOH	2-PrOH	Others	
0	1	<1	-	-	-	-	-	-
2	2	7	59	2	34	3	2	10.0
4	2	13	54	2	38	4	2	
2	5	16	69	2	24	4	1	22.8
3	5	25	67	1	26	4	2	
1	6	11	73	2	22	2	1	28.1
2	6	20	70	2	24	3	1	
1	8	12	73	1	19	4	3	36.8
2	8	26	71	2	22	4	1	

Reaction conditions: catalyst = 150 mg, glycerol = 4 g, H_2O = 2 g, *T* = 393 K. Reduction conditions: H_2 flow at 573 K (G, 573). PrD, propanediol; PrOH, propanol. Others: ethylene glycol + ethanol + propane + ethane + methane.
Note: The glycerol rate was typically calibrated by considering the glycerol conversion at 0 h with conversion level lower than 25%. The autoclave was pressurized with 1 MPa H_2 at ambient temperature to suppress side reactions during the heating to 393 K.

Table S4 Effect of glycerol concentration on glycerol hydrogenolysis over 4 wt% Ir-ReO_x/Rutile (Re/Ir = 0.24*)

Glycerol concentration / wt%	Catalyst amount / mg	Glycerol amount / g	*t* / h	Conv. / %	Selectivity / %					Conversion rate (v_g) / mmol·g-Cat^{-1} h^{-1}
					1,3-PrD	1,2-PrD	1-PrOH	2-PrOH	Others	
5	37.5	1	2	6	62	10	13	14	1	8.7*
10	75	2	2	14	69	5	17	9	0	20.3*
20	150	4	2	18	72	4	17	7	0	26.1*
40	150	4	0	<0.5	-	-	-	-	-	
			1	11	74	2	18	2	4	32.5
			2	23	71	3	21	5	0	
50	150	4	0	<0.5	-	-	-	-	-	
			1	13	73	2	19	3	3	35.2
			2	25	70	2	22	5	1	
67	150	4	0	<1	-	-	-	-	-	
			1	12	73	1	19	4	3	36.8
			2	26	71	2	22	4	1	
80	150	4	0	<1	-	-	-	-	-	
			1	14	70	2	21	3	4	38.2
			2	27	67	2	26	4	1	
100	150	4	2	15	63	2	31	3	1	21.7*

Reaction conditions: T = 393 K, $P(H_2)$ = 8 MPa. Reduction conditions: H_2 flow at 573 K (G, 573). The autoclave was pressurized with 1 MPa H_2 at ambient temperature to suppress side reactions during the heating to 393 K.
Note: Those conversion rate values with a mark (*) were calculated by only the conversion data at 2 h since the conversion at 0 h was negligible and linearity can be assumed to some extent.

Table S5 Reusability of 4 wt%-Ir Ir-ReO_x/Rutile

Re/Ir ratio	Glycerol amount / g	H_2O amount / g	Catalyst amount / mg	Usage times	Conv. / %	Selectivity / %					Conversion rate (v_g) / mmol·g-Cat^{-1} h^{-1}
						1,3-PrD	1,2-PrD	1-PrOH	2-PrOH	Others	
0.24*	1.0	19.0	150	1	24	64	5	21	8	2	17.1
0.24*	0.9	17.1	(135)[a]	2	19	64	7	18	10	1	(13.6)
0.24*	0.8	15.2	(121)[a]	3	19	65	7	16	10	2	(14.0)
0.24*	0.7	13.3	113	4	16	62	9	16	12	1	11.5
0.30*	1.0	19.0	150	1	36	59	5	26	9	1	26.3
0.30*	0.9	17.1	(135)[a]	2	30	60	6	23	9	2	(21.6)
0.30*	0.8	15.2	(121)[a]	3	28	59	8	22	9	2	(20.8)
0.30*	0.7	13.3	108	4	25	56	10	22	10	2	19.0

Reaction conditions: $P(H_2)$ = 8 MPa, T = 393 K, t = 1 h. Catalyst of 4 wt%-Ir Ir-ReO_x/Rutile (Re/Ir = 0.24*) was pre-reduced by H_2 flow at 573 K for 1 h (G, 573).

[a]Estimated amount from the final catalyst amount.

Table S6 Valence of Re determined by H_2 consumption and XRF

Catalyst	Re/Ir ratio	Ir / wt% (actual)	Re / wt% (actual)	Temperature range for calculation	Consumed H_2 / μmol	Re valence
4 wt% Ir/Rutile	-	4.0	-	323–800 K	44.2	(-0.2)[b]
4 wt% Ir/Anatase	-	4.0	-	323–700 K	42.0	(0)[b]
4 wt% Ir/P25	-	3.9	-	323–950 K	40.6	(0)[b]
0.9 wt% ReO_x/Rutile	-	-	0.7	323–550 K	9.4	2.0
4 wt%-Ir Ir-ReO_x/Rutile	0.08*(0.063)	4.0	0.3	323–750 K	44.6	3.5
	0.12* (0.13)	4.2	0.5	323–700 K	47.4	4.4
	0.24* (0.25)	3.9	0.9	323–600 K	51.5	2.5
	0.25* (0.5)	4.1	1.0	323–550 K	55.3	2.4
	0.30* (1)	4.2	1.2	323–550 K	61.7	1.5
4 wt%-Ir Ir-ReO_x/Anatase	0.16* (0.25)	3.7	0.6	323–600 K	48.4	1.0
4 wt%-Ir Ir-ReO_x/P25	0.30* (0.25)	3.9	1.2	323–800 K	49.3	4.3
4 wt%-Ir Ir-ReO_x/Rutile[a]	0.27* (0.25)	4.4	1.2	323–600 K	48.6	6.2

Molar sensitivity is defined by the H_2 consumption of Ir/SiO_2 ($IrO_2 + 2H_2 \rightarrow Ir + 2H_2O$). Sample amount of 100 mg. Re valence: 7-2 × [(amount of H_2 consumed, μmol) – 2 × (actual Ir loading amount, μmol)]/(actual Re loading amount, μmol).

[a]Precursor of $Ir(NO_3)_4$. [b]Ir valence: 4-2 × [(amount of H_2 consumed, μmol)/(actual Ir loading amount, μmol)].

Dotted line represents the baseline for H_2 consumption amount calculation.

Table S7 Results of FT-IR of adsorbed CO analysis over Ir/Rutile and Ir-ReO_x/Rutile catalysts

Catalyst	Ir loading amount (nominal) / wt%	Re/Ir ratio	Ir^0 Wavenumber / cm^{-1}	Area ratio/%	$Ir^{\delta+}$ (Ir^{3+}/Ir^{4+}) Wavenumber / cm^{-1}	Area ratio/%
Ir (G,573)	4	-	2070	65	2083	35
Ir-ReO_x (G,573)	4	0.24* (0.25)	2075	66	2089	34
Ir-ReO_x (G,573)	4	0.30* (1)	2073	68	2087	32
Ir-ReO_x (G,573)	2	0.32* (0.25)	2073	56	2083	44
Ir-ReO_x (G,573)	6	0.18* (0.25)	2074	72	2089	28
Ir-ReO_x (G,573)	8	0.15* (0.25)	2076	75	2089	25

Table S8 Dependency of Re/Ir ratio on glycerol to 1,3-PrD over 4wt%-Ir Ir-ReO_x/Rutile

Re/Ir ratio	t / h	Conv. / %	Selectivity / %					$P_{1,3\text{-PrD}}$ / g g_{Ir}^{-1} h^{-1}
			1,3-PrD	1,2-PrD	1-PrOH	2-PrOH	Others	
0.08*	0	<0.5	-	-	-	-	-	
(0.063)	4	11	73	1	19	5	2	9
	8	18	70	2	18	6	4	
0.12*	0	<0.5	-	-	-	-	-	
(0.13)	4	21	70	2	20	5	3	21
	6.7	31	67	2	23	6	2	
0.24*	0	<1	-	-	-	-	-	
(0.25)	1	12	73	1	19	4	3	52
	2	26	71	2	22	4	1	
0.25*	0	<1	-	-	-	-	-	
(0.5)	1	18	69	2	24	4	1	67
	2	32	67	2	25	5	1	
0.30*	0	<0.5	-	-	-	-	-	94
(1)	1	24	75	3	17	4	1	

Reaction conditions: catalyst = 150 mg, glycerol = 4 g, H_2O = 2 g, $P(H_2)$ = 8 MPa, T = 393 K. Reduction conditions: H_2 flow at 573 K (G, 573). The $P_{1,3\text{-PrD}}$ was calculated at glycerol conversion about 20–25%.

References

(1) Jr., J. W. C.; Sayers, D. E. Criteria for Automatic X-ray Absorption Fine Structure Background Removal. *J. Appl. Phys.* **1981,** *52*, 5024–5031.

(2) Okumura, K.; Amano, J.; Yasunobu, N.; Niwa, M. X-ray Absorption Fine Structure Study of the Formation of the Highly Dispersed PdO over ZSM-5 and the Structural Change of Pd Induced by Adsorption of NO. *J. Phys. Chem. B* **2000,** *104*, 1050–1057.

(3) Okumura, K.; Matsumoto, S.; Nishiaki, N.; Niwa, M. Support Effect of Zeolite on the Methane Combustion Activity of Palladium. *Appl. Catal. B* **2003,** *40*, 151–159.

(4) Amada, Y.; Shinmi, Y.; Koso, S.; Kubota, T.; Nakagawa, Y.; Tomishige, K. Reaction Mechanism of the Glycerol Hydrogenolysis to 1,3-Propanediol over Ir-ReO_x/SiO_2 Catalyst. *Appl. Catal. B* **2011,** *105*, 117–127.

(5) Zhu, S.; Gao, X.; Zhu, Y.; Zhu, Y.; Xiang, X.; Hu, C.; Li, Y. Alkaline Metals Modified Pt–$H_4SiW_{12}O_{40}$/ZrO_2 Catalysts for the Selective Hydrogenolysis of Glycerol to 1,3-Propanediol. *Appl. Catal. B* **2013,** *140–141*, 60–67.

(6) García-Fernández, S.; Gandarias, I.; Requies, J.; Güemez, M. B.; Bennici, S.; Auroux, A.; Arias, P. L. New Approaches to the Pt/WO_x/Al_2O_3 Catalytic System Behavior for the Selective Glycerol Hydrogenolysis to 1,3-Propanediol. *J. Catal.* **2015,** *323*, 65–75.

(7) García-Fernández, S.; Gandarias, I.; Requies, J.; Soulimani, F.; Arias, P. L.; Weckhuysen, B. M. The Role of Tungsten Oxide in the Selective Hydrogenolysis of Glycerol to 1,3-Propanediol over Pt/WO_x/Al_2O_3. *Appl. Catal. B* **2017,** *204*, 260–272.

(8) Gong, L.; Lu, Y.; Ding, Y.; Lin, R.; Li, J.; Dong, W.; Wang, T.; Chen, W. Selective Hydrogenolysis of Glycerol to 1,3-Propanediol over a Pt/WO_3/TiO_2/SiO_2 Catalyst in Aqueous Media. *Appl. Catal. A* **2010,** *390*, 119–126.

(9) Zhang, Y.; Zhao, X.-C.; Wang, Y.; Zhou, L.; Zhang, J.; Wang, J.; Wang, A.; Zhang, T. Mesoporous Ti–W Oxide: Synthesis, Characterization, and Performance in Selective Hydrogenolysis of Glycerol. *J. Mater. Chem. A* **2013,** *1*, 3724–3732.

(10) Zhu, S.; Gao, X.; Zhu, Y.; Cui, J.; Zheng, H.; Li, Y. SiO_2 Promoted Pt/WO_x/ZrO_2 Catalysts for the Selective Hydrogenolysis of Glycerol to 1,3-Propanediol. *Appl. Catal. B* **2014,** *158–159*, 391–399.

(11) Priya, S. S.; Kumar, V. P.; Kantam, M. L.; Bhargava, S. K.; Srikanth, A.; Chary, K. V. R. High Efficiency Conversion of Glycerol to 1,3-Propanediol Using a Novel Platinum–Tungsten Catalyst Supported on SBA-15. *Ind. Eng. Chem. Res.* **2015,** *54*, 9104–9115.

(12) Fan, Y. Q.; Cheng, S. J.; Wang, H.; Ye, D. H.; Xie, S. H.; Pei, Y.; Hu, H. R.; Hua, W. M.; Li, Z. H.; Qiao, M. H.; Zong, B. N. Nanoparticulate Pt on Mesoporous SBA-15 Doped with Extremely Low Amount of W as a Highly Selective Catalyst for Glycerol Hydrogenolysis to 1,3-Propanediol. *Green Chem.* **2017,** *19*, 2174–2183.

(13) Arundhathi, R.; Mizugaki, T.; Mitsudome, T.; Jitsukawa, K.; Kaneda, K. Highly Selective Hydrogenolysis of Glycerol to 1,3-Propanediol over a Boehmite-Supported Platinum/Tungsten Catalyst. *ChemSusChem* **2013,** *6*, 1345–1347.

(14) Qin, L.-Z.; Song, M.-J.; Chen, C.-L. Aqueous-Phase Deoxygenation of Glycerol to 1,3-Propanediol over Pt/WO_3/ZrO_2 Catalysts in a Fixed-Bed Reactor. *Green Chem.* **2010,** *12*, 1466–1472.

(15) Lei, N.; Zhao, X.; Hou, B.; Yang, M.; Zhou, M.; Liu, F.; Wang, A.; Zhang, T. Effective

Hydrogenolysis of Glycerol to 1,3-Propanediol over Metal-Acid Concerted Pt/WO_x/Al_2O_3 Catalysts. *ChemCatChem* **2019,** *11*, 3903–3912.

(16) Wang, J.; Zhao, X. C.; Lei, N.; Li, L.; Zhang, L. L.; Xu, S. T.; Miao, S.; Pan, X. L.; Wang, A. Q.; Zhang, T. Hydrogenolysis of Glycerol to 1,3-Propanediol under Low Hydrogen Pressure over WO_x-Supported Single/Pseudo-Single Atom Pt Catalyst. *ChemSusChem* **2016,** *9*, 784–790.

(17) Zhou, W.; Luo, J.; Wang, Y.; Liu, J. F.; Zhao, Y. J.; Wang, S. P.; Ma, X. B. WO_x Domain Size, Acid Properties and Mechanistic Aspects of Glycerol Hydrogenolysis over Pt/WO_x/ZrO_2. *Appl. Catal. B* **2019,** *242*, 410–421.

(18) Fan, Y. Q.; Cheng, S. J.; Wang, H.; Tian, J.; Xie, S. H.; Pei, Y.; Qiao, M. H.; Zong, B. N. Pt-WO_x on Monoclinic or Tetrahedral ZrO_2: Crystal Phase Effect of Zirconia on Glycerol Hydrogenolysis to 1,3-Propanediol. *Appl. Catal. B* **2017,** *217*, 331–341.

(19) Deng, C.; Duan, X.; Zhou, J.; Zhou, X.; Yuan, W.; Scott, S. L. Ir–Re Alloy as a Highly Active Catalyst for the Hydrogenolysis of Glycerol to 1,3-Propanediol. *Catal. Sci. Technol.* **2015,** *5*, 1540–1547.

(20) Liu, L.; Kawakami, S.; Nakagawa, Y.; Tamura, M.; Tomishige, K. Highly Active Iridium–Rhenium Catalyst Condensed on Silica Support for Hydrogenolysis of Glycerol to 1, 3-Propanediol. *Appl. Catal. B* **2019**, *256*, 117775.